Natural Resources Canada | Ressources naturelles Canada

GEOLOGICAL SURVEY OF CANADA
OPEN FILE 9230

U-Pb zircon geochronology of a post-kinematic, pegmatitic syenogranite dyke, northern Baffin Island, Nunavut

D.R. Skipton and N. Wodicka

2025

Canada

GEOLOGICAL SURVEY OF CANADA
OPEN FILE 9230

U-Pb zircon geochronology of a post-kinematic, pegmatitic syenogranite dyke, northern Baffin Island, Nunavut

D.R. Skipton[1] and N. Wodicka[2]

[1]Geological Survey, Department of Energy, Industry and Technology, Government of Newfoundland and Labrador, 50 Elizabeth Ave., St. John's, Newfoundland and Labrador A1A 1W6
[2]Natural Resources Canada, Geological Survey of Canada, 601 Booth Street, Ottawa, Ontario K1A 0E8

2025

This publication is available for free download through the NRCan Open Science and Technology Repository (https://ostrnrcan-dostrncan.canada.ca/).

Recommended citation
Skipton, D.R. and Wodicka, N., 2025. U-Pb zircon geochronology of a post-kinematic, pegmatitic syenogranite dyke, northern Baffin Island, Nunavut; Geological Survey of Canada, Open File 9230, 1 .zip file. https://doi.org/10.4095/pshwe86den

Publications in this series have not been edited; they are released as submitted by the author.

ISSN 2816-7155
ISBN 978-0-660-74988-4
Catalogue No. M183-2/9230E-PDF
https://doi.org/10.4095/pshwe86den

Abstract

The Geological Survey of Canada (GSC) GEM-2 North Baffin project (2017-2020) involved 1:100,000-scale bedrock mapping and associated geochronological studies of northern Baffin Island, with the aim of building on previous, less-detailed (1:250,000-scale) mapping to fill a knowledge gap in our understanding of the geology of the area. Along the northern coast of Baffin Island, southwest of the community of Pond Inlet, Neoarchean tonalitic gneiss has been thrust over Neoarchean metasedimentary rocks along the Qimivvik thrust. The thrust is cross-cut by a ~7 m wide, pegmatitic leucogranite (syenogranite) dyke, which also cross-cuts foliation in tonalitic gneiss in the hanging wall of the thrust. Uranium-Pb zircon geochronology was conducted on a sample collected from the syenogranite dyke, as the crystallization age of the dyke provides a younger age limit on the Qimivvik thrust and on foliation in the tonalitic gneiss. The dyke yielded three chemically and texturally distinct populations with various U contents, Th/U ratios, and Hf/Yb ratios. Regardless of textural/chemical population, the analyses produced equivalent dates (within errors at 95% confidence level), implying that they formed at approximately the same time during melt crystallization. The combined weighted average age of all three populations, 1809 ± 4 Ma, is considered to be the crystallization age of the dyke. Thus, movement along the Qimivvik thrust and foliation development in tonalitic gneiss in the hanging wall are interpreted to have ceased before ca. 1809 Ma.

Introduction

Northern Baffin Island (Fig. 1) was initially mapped at 1:250,000-scale in the 1960s (Jackson and Davidson, 1975; Jackson and Morgan, 1978; Jackson et al., 1978; Davidson et al., 1979), mostly conducted by helicopter-supported site visits along transects spaced ~8 km apart (Jackson, 2000). Targeted mapping of greenstone belts was conducted during 2003-2005 (Young et al., 2004; Johns and Young, 2006). However, in the absence of systematic bedrock mapping on a regional scale at a higher level of detail, and due to the scarcity of geochronological data, the geological framework of northern Baffin Island remained poorly constrained. To address this knowledge gap, 1:100,000-scale bedrock mapping was undertaken during 2017-2018 by the

GSC GEM-2 North Baffin project (Saumur et al., 2018a, 2018b, 2020a, 2020b; Skipton et al., 2018, 2020a, 2020b, 2020c), together with geochronological studies (Skipton et al., 2019, 2025; this study).

Northern Baffin Island forms part of the Rae craton and mostly comprises Archean felsic plutonic rocks, including ca. 2901-2775 Ma gneissic tonalite to granodiorite and ca. 2731-2706 Ga foliated to massive monzogranite, granodiorite, and tonalite (Figs. 1, 2; Jackson et al., 1990; Jackson, 2000; Skipton et al., 2019). Exposures of the Mary River Group greenstone belts consist of mafic volcanic rocks, siliciclastic units, banded iron formation, felsic to intermediate volcanic rocks, and ultramafic sills/volcanic rocks (e.g., Jackson, 2000; Young et al., 2004; Saumur et al., 2018c). The Mary River Group forms two temporally distinct packages, dated at ca. 2830 Ma and ca. 2760-2718 Ma (Skipton et al., 2019). In the Pond Inlet area (Fig. 2), gabbro (ca. <2720>2655 Ma), a layered mafic-ultramafic intrusion (ca. 2669 Ma), metasedimentary strata with an estimated maximum depositional age of ca. 2720 Ma, and a syenogranite intrusion (ca. 1792 Ma) are also present (Skipton et al., 2017, 2018, 2019). The Archean rocks of northern Baffin Island have been regionally metamorphosed at predominantly amphibolite-to-granulite facies conditions, and at least three regional deformation events have produced strongly foliated rocks that are complexly folded (for details, the reader is referred to Jackson, 2000; Young et al., 2004; Skipton et al., 2017, 2025; Saumur et al., 2018c).

This report presents U-Pb zircon geochronology determined on a sample from a pegmatitic syenogranite dyke from the Qimivvik area on northern Baffin Island (Fig. 2). In the Qimivvik area, Archean tonalitic gneiss (ca. 2706 Ma) has been juxtaposed over Archean metasedimentary rocks (with a loosely constrained maximum depositional age of ca. 2.7 Ga) by the Qimivvik thrust (Skipton et al., 2017, 2019, 2025). The thrust is cross-cut by a series of pegmatitic leucogranite (syenogranite) dykes (Fig. 3a), and the dykes cross-cut foliation in the tonalite gneiss in the hanging wall of the thrust. As such, determining the age of one of these pegmatitic syenogranite dykes should provide a younger age constraint on the timing of thrusting and foliation development. In the footwall of the thrust, outcrop exposures showing the relationships between the dykes and the host rocks (pelite) are limited to inaccessible vertical cliff exposures, but remote observations (by helicopter and zoom photography) suggest that the dykes are connected to a network of leucogranite within the pelite (Fig. 3a).

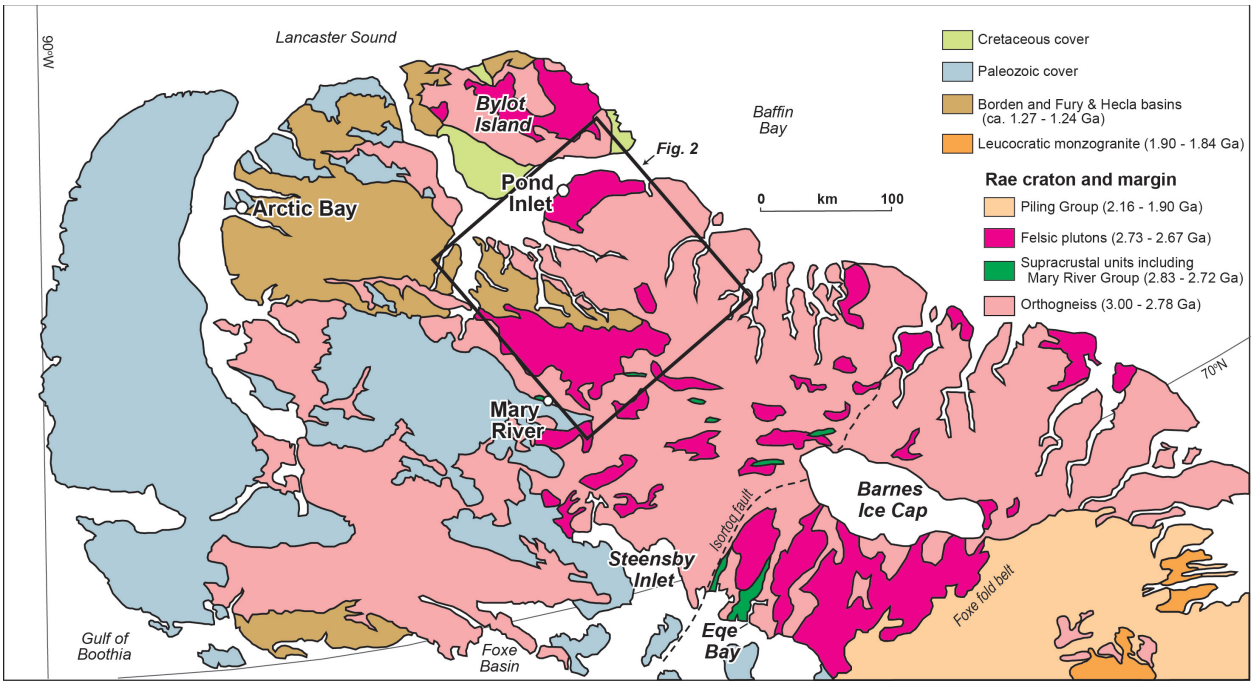

Fig. 1: Generalized geological map of northern Baffin Island (modified after St-Onge et al., 2020). The black outline indicates the area shown in Figure 2.

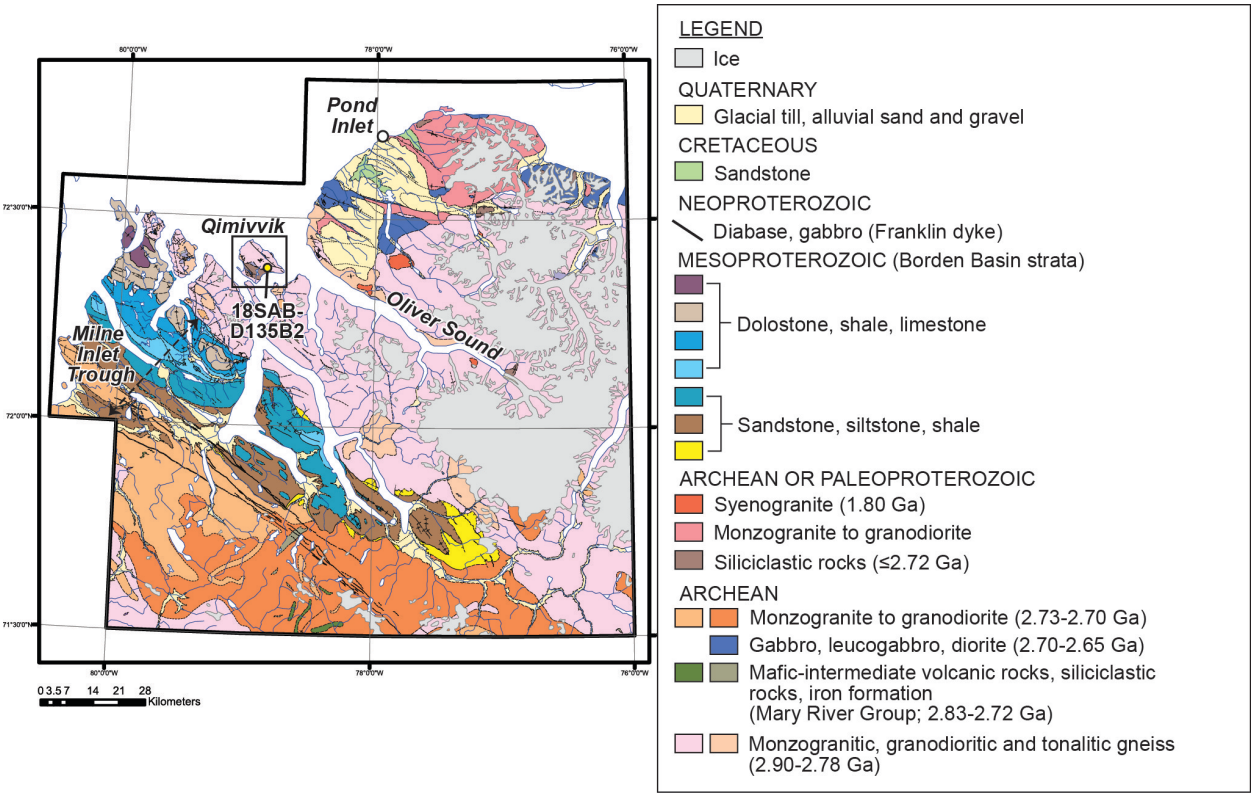

Fig. 2 (previous page): Simplified geological map of the Pond Inlet area of northern Baffin Island (from Saumur et al., 2018a, Skipton et al., 2018). The black square shows the location of the Qimivvik area and the yellow circle indicates the location of U-Pb zircon geochronology sample 18SAB-D135B2.

Methods

Uranium-Pb zircon geochronology was conducted using the sensitive high-resolution ion microprobe (SHRIMP) at the J.C. Roddick Ion Microprobe facility at the GSC (Ottawa, Ontario). The sample was processed using standard crushing, Wilfley table, magnetic, and heavy-liquid separation techniques, and analyzed on a SHRIMP II instrument following the analytical procedures of Stern (1997) and Stern and Amelin (2003). Zircon grains were hand-picked to select the highest-quality grains and representative morphological varieties. Zircon were mounted in a 2.5 cm diameter epoxy mount (IP# 943), together with reference materials. Zircon z6266 was used as the primary reference material ($^{206}Pb/^{238}U$ age = 559 ± 0.2 Ma; Stern and Amelin, 2003) and zircon z1242 as the secondary reference material ($^{207}Pb/^{206}Pb$ age = 2679.7 ± 0.2 Ma; Davis et al., 2019). Using 9, 6, and 1 μm diamond compound, the mount was polished to reveal the middle of the zircon grains.

Back-scattered electron (BSE) images of internal features such as zoning, structures, and alteration were acquired using a Zeiss EVO 50 Scanning Electron Microscope (SEM) at the GSC (Ottawa, Ontario). Mount surfaces were evaporatively coated with 10 nm of high purity Au. Each SHRIMP analysis involved a set of 6 scans over 11 isotope masses of Zr^+, U^+, Pb^+, Th^+, Yb^+, and Hf^+ sequentially measured with a single electron multiplier corrected for a deadtime of 21 ns. A $^{16}O-$ primary beam was used with a spot size of ~12 μm, a depth of ~1 μm, and a beam current of ~3.6 nA. Both reference materials were analyzed on the same mount and under the same conditions as the unknowns. The data were processed offline using SQUID2 software (v. 2.50.11.10.15, rev. 15 Oct. 2011; Ludwig, 2009). Decay constants follow the recommendations of Steiger and Jäger (1977). The 1σ external errors of $^{206}Pb/^{238}U$ ratios incorporate a ±1.00% error in calibrating the primary zircon reference material (see Stern and Amelin, 2003). Analyses of the secondary reference material z1242 were interspersed between the sample analyses to monitor accuracy of the measured $^{207}Pb/^{206}Pb$ ratios and correct for any instrumental mass bias.

No fractionation correction was applied to the Pb-isotope data. The Pb composition of the surface blank was used to correct for ^{204}Pb following the methods of Stern (1997). Yb and Hf concentration data were calculated using sensitivity factors derived from z6266 with values of 229 and 8200 ppm, respectively. Corrected ratios and ages are reported with 1σ analytical errors (68% confidence) in Appendix 1, together with further details of analytical conditions. Isoplot v. 4.15 (Ludwig, 2012) was used to generate the concordia plot and calculate weighted means. The error ellipses on the concordia diagram and the weighted mean errors are reported at the 95% confidence level. All zircon dates and calculated ages reported herein are ^{207}Pb/^{206}Pb ages.

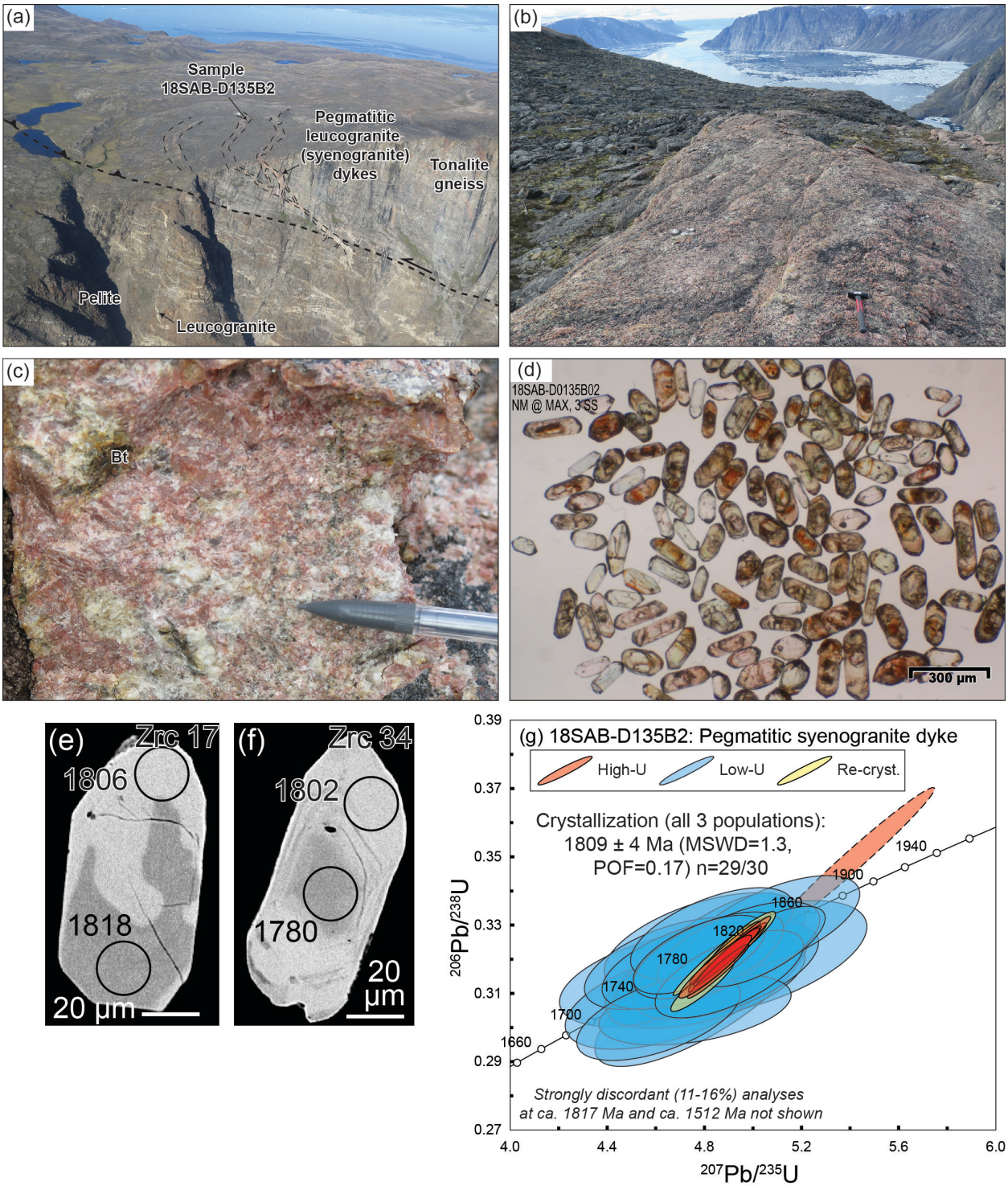
(a)
Sample
18SAB-D135B2
Pegmatitic
leucogranite
(syenogranite)
dykes
Tonalite
gneiss
Pelite
Leucogranite
(b)
(c)
Bt
(d)
18SAB-D0135B02
NM @ MAX, 3° SS
300 µm
(e)
Zrc 17
1806
1818
20 µm
(f)
Zrc 34
1802
1780
20
µm
(g) 18SAB-D135B2: Pegmatitic syenogranite dyke
High-U
Low-U
Re-cryst.
Crystallization (all 3 populations):
1809 ± 4 Ma (MSWD=1.3,
POF=0.17) n=29/30
1940
1900
1860
1820
1780
1740
1700
1660
Strongly discordant (11-16%) analyses
at ca. 1817 Ma and ca. 1512 Ma not shown
0.39
0.37
0.35
0.33
0.31
0.29
0.27
206Pb/238U
4.0
4.4
4.8
5.2
5.6
6.0
207Pb/235U

Fig. 3 (previous page): (a) Cliff exposure of the east-northeast-dipping Qimivvik thrust (black dashed line with thrust teeth), which juxtaposes Neoarchean tonalite gneiss over Neoarchean pelite and psammite. White-to-pink coloured leucogranite (syenogranite) dykes cross-cut the thrust, and also appear to be connected to leucogranite in cliff exposures of pelite in the footwall. Sample 18SAB-D135B2 was collected from one of these dykes, as indicated. NRCan Photo 2023-736. (b) The pegmatitic leucogranite (syenogranite) dyke from which sample 18SAB-D135B2 was collected (pink-orange-coloured, in foreground), surrounded by host rocks consisting of dark grey weathered tonalitic gneiss. NRCan Photo 2023-737. (c) Fresh surface of geochronology sample 18SAB-D135B2, composed of mainly K-feldspar, plagioclase, and quartz, with minor biotite. NRCan Photo 2023-738. All field photos by D. Skipton. (d–f) Representative images of zircon from sample 18SAB-D135B2, taken in transmitted light (d) and back-scattered electron mode (e, f). Black circles indicate SHRIMP spot locations, which are each labelled with the corresponding $^{207}Pb/^{206}Pb$ date (in Ma). (g) Concordia plot showing SHRIMP U-Pb zircon data and calculated age for sample 18SAB-D135B2. The age is reported as a $^{207}Pb/^{206}Pb$ weighted average age (95% confidence level uncertainty). Red ellipse with dashed outline corresponds to analysis 12402-65.1, which was statistically rejected from the weighted average age (of all 3 populations) based on the outlier criterion of Ludwig (2012) (refer to text for details).

Results and Interpretation

Sample 18SAB-D135B2 (lab number 12402) was collected from a 7 m-wide pegmatitic leucogranite (syenogranite) dyke that is massive, pink–orange-weathered, dips moderately toward the east-southeast, and cross-cuts foliation in the host tonalite gneiss in the hangingwall of the Qimivvik thrust (Fig. 3a, b). The sample is mainly composed of coarse-grained to pegmatitic quartz, K-feldspar, and plagioclase, and minor, partially to fully chloritized biotite (Fig. 3c).

Zircon grains in sample 18SAB-D135B2 occur mostly as brown, prismatic crystals commonly with inclusion-rich, fractured cores surrounded by clear rims (Fig. 3d). A subset of clear, colourless, inclusion-poor, subequant to prismatic grains is also present (Fig. 3d). BSE images reveal the presence of highly altered oscillatory zoned (not shown) or dark homogeneous

to faintly zoned cores surrounded by bright or oscillatory zoned rims (Fig. 3e, f), as well as dark, faintly zoned, or homogeneous grains (not shown). Both oscillatory zoned and faintly zoned to homogenous grains are typically cut by highly irregular, bright zones interpreted as recrystallization or dissolution/reprecipitation fronts (Fig. 3e). Thirty-two analyses were conducted on 30 zircon crystals, comprising at least three chemically and texturally distinct populations: 1) dark-BSE homogeneous or faintly zoned cores and grains have relatively low U contents (22-95 ppm), high Th/U ratios (1.31-1.92), and high Hf/Yb ratios (65-157); 2) bright-BSE and oscillatory-zoned rims have very high U contents (1155-1544 ppm with one grain as high as 3778 ppm), relatively low Th/U ratios (0.04-0.19), and low/uniform Hf/Yb ratios (17-46); and 3) irregular, bright zones have intermediate U contents (538-867 ppm with one exception at 2049 ppm) and Hf/Yb ratios (40-114), and relatively low Th/U ratios (0.08-0.18) (Appendix 1). No analyses were conducted on oscillatory zoned cores because of strong alteration. The low-U cores (4 spots) and whole crystals (15 spots) produced a weighted average age of 1802 ± 19 Ma (MSWD=0.86, POF=0.63; blue ellipses in Fig. 3g). The high-U, bright or oscillatory-zoned rims, comprising 7 analyses on 7 grains, yielded a weighted average age of 1810 ± 11 Ma (MSWD=5.1, POF=0.000; red ellipses in Fig. 3g). Analyses from bright recrystallized zones (4 spots on 4 grains) gave a very similar weighted average age of 1812 ± 8 Ma (MSWD=0.55, POF=0.65; yellow ellipses in Fig. 3g). Two analyses (12402-093.1 and -029.1) are excluded from age calculations due to significant discordance (≥11%) and high ^{204}Pb.

The equivalent (within errors at 95% confidence level) ages of the texturally and chemically distinct zircon populations suggest that they formed at approximately the same time during melt crystallization. Thus, the combined weighted average age of all three populations, 1809 ± 4 Ma (n = 29/30; MSWD=1.3, POF=0.17), is considered to be a reasonable estimate of the crystallization age of the syenogranite dyke. Analysis 12402-065.1 with a ^{207}Pb/^{206}Pb date of 1840 ± 8 Ma was statistically rejected based on Ludwig's (2012) modified 2-sigma approach for outlier rejection.

Considering the field relationships of the dyke from which the sample was collected (described above), the geochronological data indicate that the Qimivvik thrust, as well as foliation development in the tonalitic gneiss that hosts the dyke, occurred prior to ca. 1809 Ma. The age of the dyke is similar to the 1792 ± 3 Ma age (Skipton et al., 2019) of a ~10 km-wide, post-kinematic syenogranite pluton located to the east, south of Pond Inlet (Fig. 2), suggesting

that ca. 1.8 Ga felsic magmatism may have occurred over a broad region on northern Baffin Island, although it appears to have produced relatively small and sparsely-distributed intrusions.

Acknowledgements

This work was financially supported by the GSC GEM-2 North Baffin project (2017-2020). DRS was supported by the GSC's Alice Wilson Postdoctoral Fellowship. The authors thank the GEM-2 North Baffin bedrock mapping team for their contributions to understanding the geology of the study area. Sabrina Chan and Quinn Emon are thanked for their help in preparing the grain mount. The authors are grateful to Meghan Moher for acquiring SEM images and to Nicole Rayner and Tom Pestaj for their insights and help in the SHRIMP lab. Nicole Rayner is thanked for her critical review of the manuscript.

References

Davidson, A., Jackson, G.D., and Morgan, W.C., 1979. Geology, Icebound Lake, District of Franklin; Geological Survey of Canada, Map 1451A, coloured, with expanded legend, scale 1:250 000. https://doi.org/10.4095/109161

Davis, W.J., Pestaj, T., Rayner, N., and McNicoll, V.M., 2019. Long-term reproducibility of $^{207}Pb/^{206}Pb$ age at the GSC SHRIMP lab based on the GSC Archean reference zircon z1242. Geological Survey of Canada, Scientific Presentation 111, 1 poster, https://doi.org/10.4095/321203

Jackson, G.D., 2000. Geology of the Clyde-Cockburn Land map area, north-central Baffin Island, Nunavut; Geological Survey of Canada, Memoir 440, 316 p. https://doi.org/10.4095/211268

Jackson, G.D. and Davidson, A., 1975. Geology, Pond Inlet and Nova Zembla Island, District of Franklin; Geological Survey of Canada, Map 1396A, coloured, with expanded legend, scale 1:250 000. https://doi.org/10.4095/109005

Jackson, G.D. and Morgan, W.C., 1978. Geology, Conn Lake, District of Franklin; Geological Survey of Canada, Map 1458A, coloured, with expanded legend, scale 1:250 000. https://doi.org/10.4095/109162

Jackson, G.D., Morgan, W.C., and Davidson, A., 1978. Geology, Steensby Inlet, District of Franklin; Geological Survey of Canada, Map 1450A, coloured, with expanded legend, scale 1:250 000. https://doi.org/10.4095/109160

Jackson, G.D., Hunt, P.A., Loveridge, W.D., and Parrish, R.R., 1990. Reconnaissance geochronology of Baffin Island, N.W.T.; in Radiogenic Age and Isotopic Studies: Report 3, Geological Survey of Canada Paper 89-2, p. 123–148. https://doi.org/10.4095/129079

Johns, S.M. and Young, M.D., 2006. Bedrock geology and economic potential of the Archean Mary River group, northern Baffin Island, Nunavut; Geological Survey of Canada Current Research 2006-C5, 13 p. https://doi.org/10.4095/222954

Ludwig, K.R., 2009. SQUID 2: A User's Manual, rev. 12 Apr, 2009. Special Publication 5, Berkeley Geochronology Center, Berkeley 110 p.

Ludwig, K.R., 2012. Isoplot 3.75–4.15, A geochronological toolkit for Microsoft Excel: Berkeley Geochronology Center Special Publication No. 5, 75 p.

Saumur, B.M., Skipton, D.R., St-Onge, M.R., Wodicka, N., Bros, E.R., and Weller, O.M., 2018a. Bedrock geology, Mumiksaa-Milne Inlet, Nunavut, parts of NTS 38-B and 48-A. Geological Survey of Canada, Canadian Geoscience Map 348, scale 1:100 000, 1 sheet. https://doi.org/10.4095/306579

Saumur, B.M., Skipton, D.R., St-Onge, M.R., Wodicka, N., Bros, E.R., and Weller, O.M., 2018b. Bedrock geology, Kanajuqtuuq (Paquet Bay), Nunavut, NTS 37-G north. Geological Survey of Canada, Canadian Geoscience Map 349, scale 1:100 000, 1 sheet. https://doi.org/10.4095/306584

Saumur, B.M., Skipton, D.R., St-Onge, M.R., Bros, E.R., Acosta-Gongora, P., Kelly, C.J., Morin, A., O'Brien, M.E., Johnston, S.T., and Weller, O.M., 2018c. Precambrian geology of the surroundings of Steensby Inlet and western Barnes Ice Cap (parts of NTS37E, 37F, 37G), Baffin Island, Nunavut; in Summary of Activities 2018, Canada-Nunavut Geoscience Office, p. 29–46.

Saumur, B.M., Skipton, D.R., St-Onge, M.R., Jackson, G.D., Wodicka, N., Bros, E.R., Weller, O.M., and Johnston, S.T., 2020a. Bedrock geology, Angijurjuk-Mary River, Baffin Island, Nunavut, NTS 37-G west. Geological Survey of Canada, Canadian Geoscience Map 403, scale 1:100 000, 1 sheet. https://doi.org/10.4095/321794

Saumur, B.M., Skipton, D.R., Zhang, S., St-Onge, M.R., Bros, E.R., Acosta-Gongora, P., Kelly, C.J., O'Brien, M.E., Weller, O.M., and Johnston, S.T., 2020b. Bedrock geology, Nina Bang Lake, Baffin Island, Nunavut, NTS 37-F west and part of 37C-west. Geological Survey of Canada, Canadian Geoscience Map 404, scale 1:100 000, 1 sheet. https://doi.org/10.4095/314876

Skipton, D.R., Saumur, B.M., St-Onge, M.R., Wodicka, N., Bros, E.R., Morin, A., Brouillette, P., Weller, O.M., and Johnston, S.T., 2017. Precambrian bedrock geology of the Pond Inlet–Mary River area, northern Baffin Island, Nunavut; in Summary of Activities 2017, Canada-Nunavut Geoscience Office, p. 49–68.

Skipton, D.R., Saumur, B.M., St-Onge, M.R., Wodicka, N., Bros, E.R., Currie, L.D., Haggart, J.W., and Weller, O.M., 2018. Bedrock geology, Pond Inlet, Nunavut, part of NTS 38-B. Geological Survey of Canada, Canadian Geoscience Map 347, scale 1:100 000, 1 sheet. https://doi.org/10.4095/306578

Skipton, D.R., Wodicka, N., McNicoll, V., Saumur, B.M., St-Onge, M.R., and Young, M.D., 2019. U-Pb zircon geochronology of Archean greenstone belts (Mary River Group) and surrounding Archean to Paleoproterozoic rocks, northern Baffin Island, Nunavut. Geological Survey of Canada Open File 8585. https://doi.org/10.4095/314938

Skipton, D.R., Saumur, B.M., St-Onge, M.R., Bros, E.R., Acosta-Gongora, P., Kelly, C.J., O'Brien, M.E., Weller, O.M., and Johnston, S.T., 2020a. Bedrock geology, Barnes Ice Cap northwest, Baffin Island, Nunavut, NTS 37-E west. Geological Survey of Canada, Canadian Geoscience Map 402, scale 1:100 000, 1 sheet. https://doi.org/10.4095/314657

Skipton, D.R., Saumur, B.M., St-Onge, M.R., Bros, E.R., Acosta-Gongora, P., Kelly, C.J., O'Brien, M.E., Weller, O.M., and Johnston, S.T., 2020b. Bedrock geology, Rowley River-Isortoq River, Baffin Island, Nunavut, 37-F east. Geological Survey of Canada, Canadian Geoscience Map 406, scale 1:100,000, 1 sheet. https://doi.org/10.4095/315401

Skipton, D.R., Saumur, B.M., St-Onge, M.R., Wodicka, N., Bros, E.R., and Weller, O.M., 2020c. Bedrock geology, Ravn River, Baffin Island, Nunavut, NTS 37-G east. Geological Survey of Canada, Canadian Geoscience Map 405, scale 1:100 000, 1 sheet. https://doi.org/10.4095/323660

Skipton, D.R., Wodicka, N., Weller, O., Jackson, S., St-Onge, M.R., Saumur, B., and Petts, D., 2025. Polyphase metamorphism of the northern Rae craton (Baffin Island, Arctic Canada) and trace element behaviour in monazite: insights from phase equilibria modelling and geochronology. Journal of Metamorphic Geology, v. 43, p. 287–314. https://doi.org/10.1111/jmg.12808

Steiger, R.H. and Jäger, E., 1977. Subcommission on geochronology: Convention on the use of decay constants in geo- and cosmochronology. Earth and Planetary Science Letters, v. 36, p. 359–362. https://doi.org/10.1016/0012-821X(77)90060-7

Stern, R.A., 1997. The GSC Sensitive High Resolution Ion Microprobe (SHRIMP): analytical techniques of zircon U-Th-Pb age determinations and performance evaluation: *in* Radiogenic Age and Isotopic Studies, Report 10, Geological Survey of Canada, Current Research 1997-F, p. 1–31. https://doi.org/10.4095/209089

Stern, R.A. and Amelin, Y., 2003. Assessment of errors in SIMS zircon U-Pb geochronology using a natural zircon standard and NIST SRM 610 glass. Chemical Geology, v. 197, p. 111–146. https://doi.org/10.1016/S0009-2541(02)00320-0

St-Onge, M.R., Scott, D.J., Rayner, N., Sanborn-Barrie, M., Skipton, D.R., Saumur, B.M., Wodicka, N., and Weller, O.M., 2020. Archean and Paleoproterozoic Cratonic Rocks of Baffin Island. In "Geological Synthesis of Baffin Island (Nunavut) and the Labrador-Baffin Seaway", (ed.) L.T. Dafoe and N. Bingham-Koslowski. Geological Survey of Canada Bulletin, 608, 29 p. https://doi.org/10.4095/321824

Young, M.D., Sandeman, H., Berniolles, F., and Gertzbein, P.M., 2004. A preliminary stratigraphic and structural geology framework of the Archean Mary River Group, northern Baffin Island, Nunavut; Geological Survey of Canada, Current Research 2004-C1, 14 p. https://doi.org/10.4095/215376